Simulation of Shielding Performance Against Near Field Coupling to EMI Filter for Power Electronic Converter using FEM

Keita Takahashi[1], Yuichiro Murata[1], Yusuke Tsubaki[2], Tetsuro Fujiwara[3], Hideto Maniwa[2], and Naohisa Uehara[2]
[1] Mitsubishi Electric Corporation, Advanced Technology R&D Center, Amagasaki, Japan
Takahashi.Keita@df.MitsubishiElectric.co.jp
[2] Mitsubishi Electric Corporation, Automotive Electronics Development Center, Himeji, Japan
[3] Mitsubishi Electric Engineering Co., Ltd., Himeji Engineering Office, Himeji, Japan

***Abstract*—When designing an Electromagnetic interference (EMI) filter for power electronic converters, we should consider the shielding performance against the external near field coupling to the EMI filter as well as the attenuation performance. In this paper, we studied the validity of the Finite Element Method (FEM) simulation of the EMI filter for predicting the shielding performance before a trial manufacture. First, we created models of capacitors and common mode choke coils which can simulate their impedance characteristics. Next, using these component models, the assembled EMI filter model was created. We compared the measured and simulated results to verify the model. The shielding performance was evaluated using a loop coil as an external near field source. Consequently, the simulated results agreed with the measured results well.**

Keywords—power electronic converter; EMI filter; shield; FEM simulation.

I. INTRODUCTION

Electromagnetic interference (EMI) generated by power electronic converters is increasing as the frequency and the speed of semiconductor switching is getting higher [1]. Although the high frequency and high speed switching contributes to downsizing converters, EMI filters are required to reduce the large EMI noise with the small space. It is a well known fact that parasitic elements in the EMI filter play important roles in the filter performance [2]–[7].

The filter performance will be degraded by external near field couplings as well as by the internal parasitic elements. In particular, when an EMI filter is positioned close to the EMI source such as switching devices, cables, or busbars, the EMI filter will be exposed to the near field generated by them. Therefore, the EMI filter needs a shield against the external near field. Moreover, we should shield only a necessary part of the EMI filter rather than the whole of the EMI filter to minimize the filter size. However, it is difficult to optimize the shielding design by trial and error manufacturing. The goal of this work is to design the shielding by the prediction of the shielding performance before a trial manufacture. In this paper, we studied the validity of the shielding simulation of the EMI filter using Finite Element Method (FEM). For simplicity, a loop coil was used as an external near field source. The coupling factor between the coil and the filter was evaluated using S parameter. Measured and simulated results were compared to verify the simulation model. We used CST Microwave Studio® Frequency Domain Solver, which is based on FEM [8].

II. MODELING OF EMI FILTER COMPONENTS

A. Circuit of Studied EMI Filter

The circuit of the studied EMI filter is shown in Fig. 1. It consists of three X capacitors (C_{X1}, C_{X2}, C_{X3}), two pairs of Y capacitors (C_{Y1}, C_{Y2}), two common mode choke coils (L_{CMC1}, L_{CMC2}), and a varistor. L_{CMC1} and L_{CMC2} are the same. C_{Y1} and C_{Y2} are the same. C_{X1} and C_{X2} are the same. This EMI filter was designed to reduce the conducted EMI lower than CISPR 14-1 limit for the frequency range 150 kHz to 30 MHz.

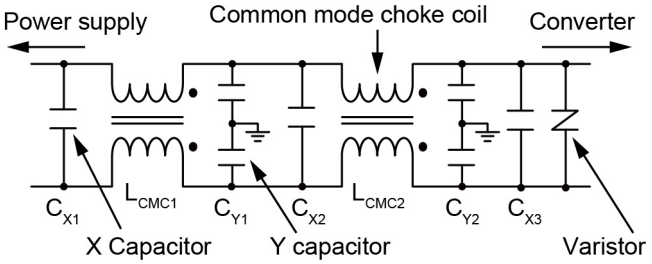

Fig. 1. Circuit of studied EMI filter.

B. Modeling of Capacitors

A simulation model of a capacitor for C_{X1} and C_{X2} is shown in Fig. 2. The capacitor model consists of two infinitely thin perfect conductor sheets, two thin dielectrics, a normal conductor, and two lead wires. The two thin dielectrics are positioned on two opposite sides of the normal conductor. The two perfect conductor sheets are on the two outer faces of the dielectrics. Similarly, the other capacitors are modeled. We considered the varistor as a capacitor since it behaves like a capacitor at low voltages. The parameters of the capacitor models are shown in Table I. Since a capacitor and a measurement port are mounted on a printed circuit board (PCB), the PCB is also modeled. Relative permittivity of the

978-1-5090-1416-3/16/$31.00 ©2016 IEEE

board is 4.7. The width and the thickness of the patterns are 1 mm and 0.1 mm, respectively. The impedance was calculated from the reflection S11.

Figure 3 shows the measured and simulated impedance of the capacitors. The impedance was measured using a network analyzer Agilent E5061B. The simulated impedance at the capacitive region where the frequency is lower than the resonance point agrees with the measurement by adjusting permittivity of the dielectrics. The simulated impedance at the resonance frequency, which is so-called series resistance, agrees with the measurement by adjusting conductivity of the normal conductor. The simulated impedance at the inductive region where the frequency is higher than resonance point agrees with the measurement without adjusting any parameters.

TABLE I. PARAMETERS OF CAPACITOR MODELS

Capacitor	*Thickness of dielectric*	*Relative permittivity of dielectric*	*Conductivity of normal conductor*
C_{X3}	0.5 mm	4.64×10^5	8071 S/m
C_{X1}, C_{X2}	0.5 mm	3.49×10^5	5721 S/m
C_{Y1}, C_{Y2}	0.2 mm	2.70×10^3	199 S/m
Varistor	0.2 mm	1.12×10^2	260 S/m

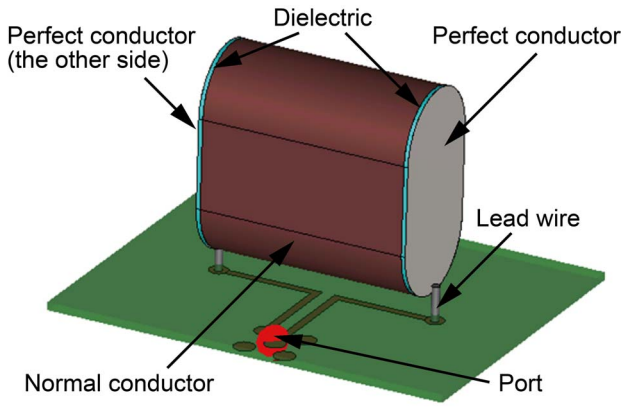

Fig. 2. Simulation model of a capacitor for C_{X1} and C_{X2}.

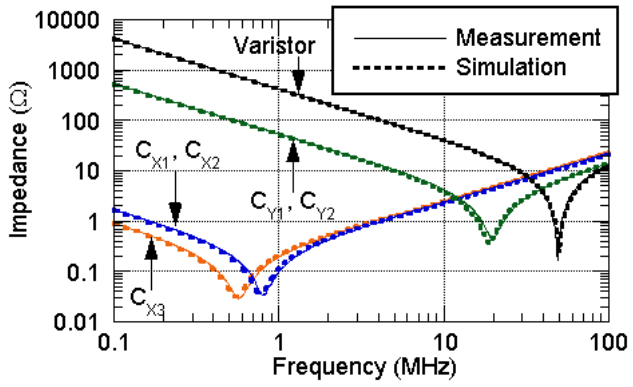

Fig. 3. Measured and simulated impedance of capacitors.

C. Modeling of Common Mode Choke Coil

A simulation model of a common mode choke coil is shown in Fig. 4. The coil model consists of an artificial dielectric, a core, a core case, and two coil windings. The relative permittivity of the core case is 4.8. In order to avoid self-intersections of the coil windings, the clearance between coil turns of the model is made to be larger than that of the actual coil. For this reason, the artificial dielectric fills the clearance to increase the parasitic capacitance between turns in the model. The relative permittivity of the artificial dielectric is 2.5. The impedance measurement method is similar to the method for capacitors.

The measured coil has a Finemet® toroidal core [9]. Since modeling all rolled thin nanocrystalline ribbon is not realistic, the core model consists of five infinitely thin surface impedance sheets and a toroidal magnetic solid. The surface impedance sheets simulate eddy current losses generated by leakage magnetic flux. The magnetic solid simulates the circumferential magnetic flux in the core. A surface impedance sheet is on the inner curved face of the magnetic solid. Another sheet is on the outer curved face. The other three sheets are positioned between the outer and the inner curved face of the core. The magnetic solid has complex permeability ($\mu' - j\mu''$). Figure 5 shows measured relative complex permeability of the core.

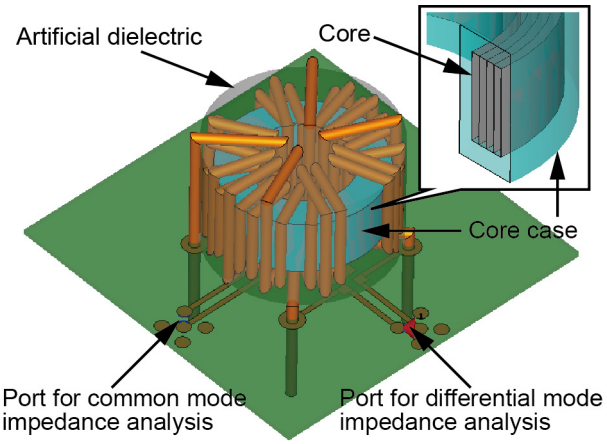

Fig. 4. Simulation model of a common mode choke coil.

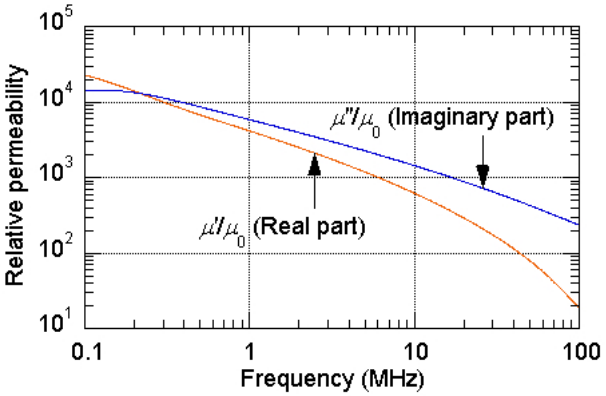

Fig. 5. Measured relative complex permeability of a core.

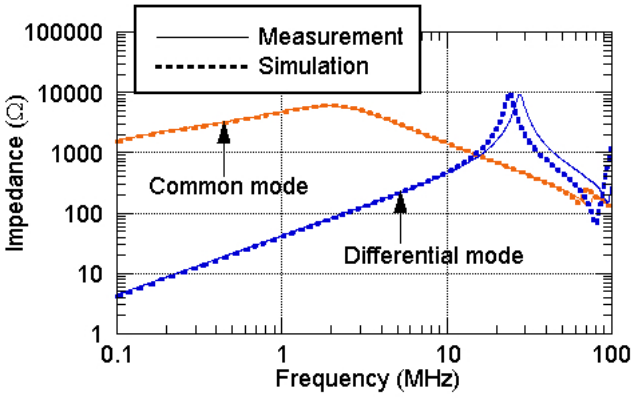

Fig. 6. Measured and simulated impedance of a common mode choke coil.

Actually, adjacent nanocrystalline layers in the toroidal core are insulated by epoxy layer whose relative permittivity is about 3.3. The total thickness of the insulator is about 1/4 of the thickness of the core. Hence, relative permittivity of the magnetic solid is 13.2 (=3.3×4) to simulate the capacitive characteristic inside the core in the radial direction. Surface impedance Z of the surface impedance sheet is shown in (1) [10]. σ is conductivity (=1/(1.2×10^{-6}) S/m) [11]. f is frequency. Complex permeability ($\mu' - j\mu''$) in (1) is similar to that of the magnetic solid. Figure 6 shows the measured and simulated impedance of the common mode choke coil. The simulated impedance agrees with the measurement well.

$$Z = (1+j)\sqrt{\pi f(\mu' - j\mu'')/\sigma} \qquad (1)$$

Although the modeling of capacitors and coils requires impedance measurements, already created models can be reused for other filters unless the capacitor and the coil are changed. Even if impedance measurements are needed, it will not take long time.

III. Attenuation Performance of EMI Filter

We assembled capacitors, common mode coke coils, and busbars on an aluminum base plate as shown in Fig. 7. Figure 8 shows the simulation model of the assembled EMI filter, which includes the component models shown in II. Using a four ports network analyzer Agilent E5071B, we measured mixed-mode S parameters of the EMI filter. Port 1 consists of two single-ended ports. Port 2 consists of two single-ended ports as well. Port 1 is at the terminals for connection to converter. Port 2 is at the terminals for connection to power supply. The EMI filter can be shielded with an aluminum plate.

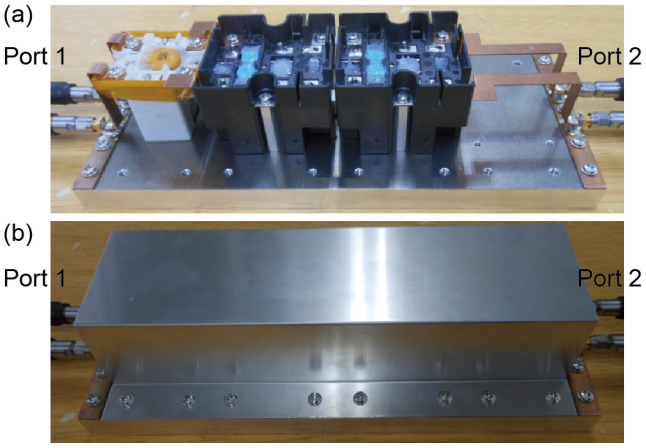

Fig. 7. Photo of an assembled EMI filter. (a) without shield (b) with shield.

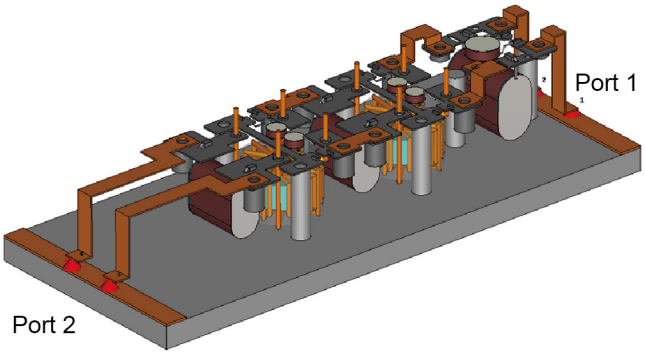

Fig. 8. Simulation model of an assembled EMI filter.

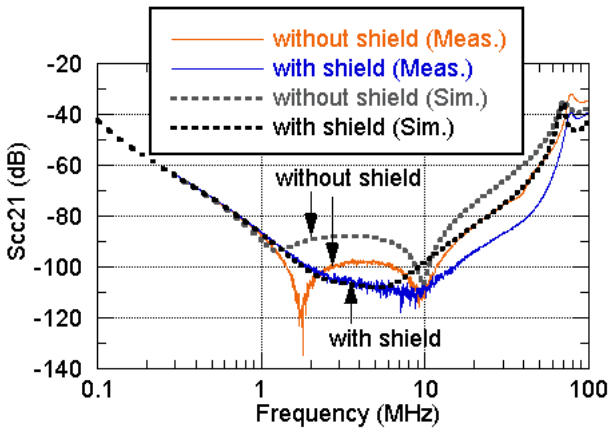

(a) Common mode attenuation

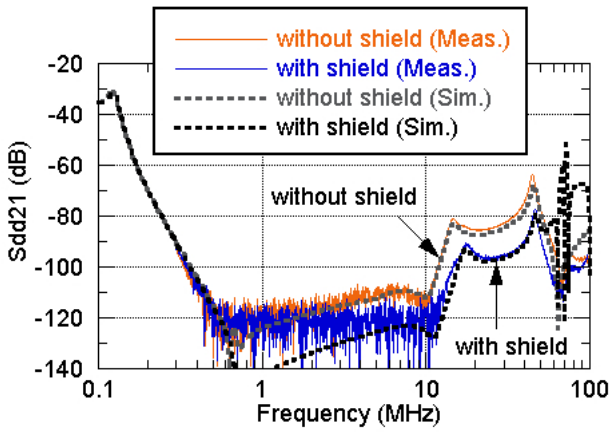

(b) Differential mode attenuation

Fig. 9. Attenuation performance of an EMI filter. (Solid lines show measurements. Dotted lines show simulations.)

The attenuation performance of the assembled EMI filter is shown in Fig. 9. Figure 9(a) shows Scc21, which means how much a common mode source signal excited at port 1 propagates to port 2 as a common mode signal. Figure 9(b) shows Sdd21, which means how much a differential mode source signal excited at port 1 propagates to port 2 as a differential mode signal.

Simulated Sdd21 agrees with the measurement within 5 dB at the frequency lower than 50 MHz except the level lower than the noise floor -115 dB. Both measured and simulated Sdd21 at the frequency above 1 MHz are reduced about 10~15 dB by the shield. Simulated Scc21 agrees with the measurement at the frequency lower than 1 MHz well. However, there is 10~30 dB difference between measured and simulated Scc21 above 1 MHz. The difference is probably caused by coaxial cables connected to port 1 and port 2, which are not considered in the simulation. Nevertheless, the model is enough to evaluate the shielding performance since the simulated Scc21 substantially agree with the measurement.

IV. Shielding Performance Against External Near Field Coupling to EMI Filter

Photo of the EMI filter with a PCB loop coil is shown in Fig. 10. The PCB loop coil has a one-turn pattern and generates near field by a source signal excited from a single-ended port 1. The generated near field couples with the EMI filter. Consequently, a coupling signal propagates to port 2. Port 2 consists of two single-ended ports. Port 2 is at the terminals for connection to power supply. The terminals for connection to converter are 50 ohm terminated. Using a four ports network analyzer Agilent E5071B, we measured mixed-mode S parameters; Scs21 and Sds21. Scs21 means how much a common mode coupling signal propagates to port 2. Sds21 means how much a differential mode coupling signal propagates to port 2.

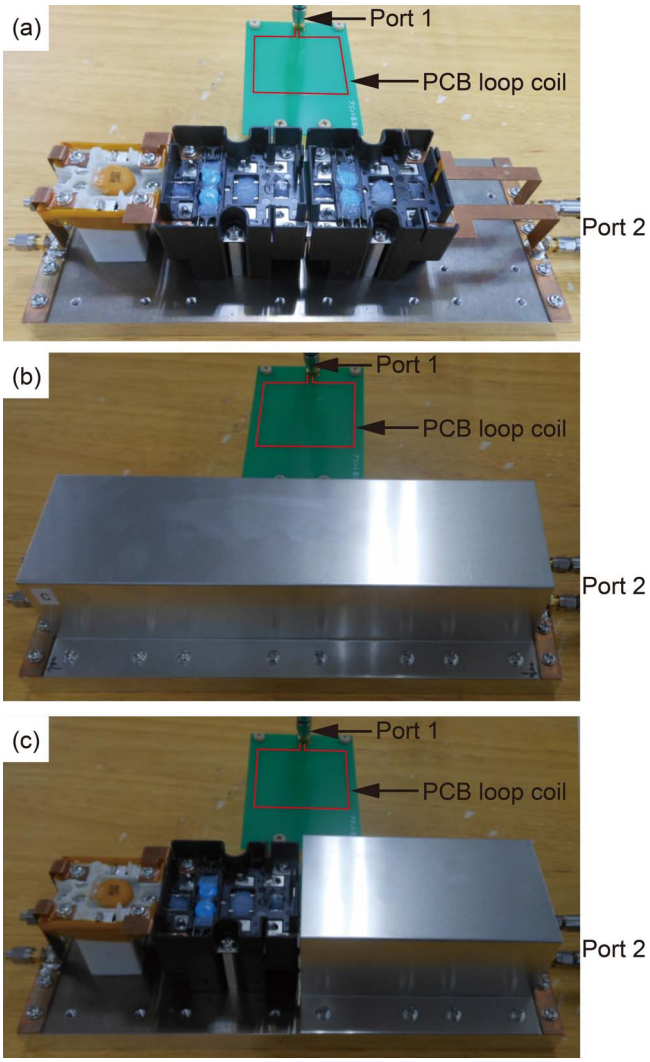

Fig. 10. Photo of an EMI filter with a PCB loop coil. (a) without shield (b) with full shield (c) with partial shield.

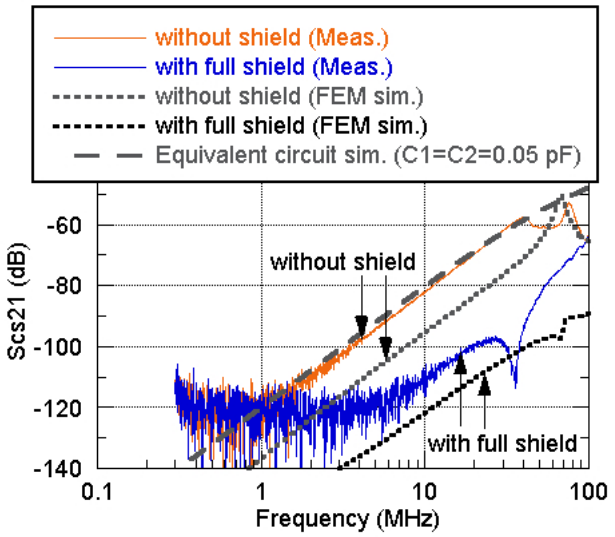

(a) Common mode coupling

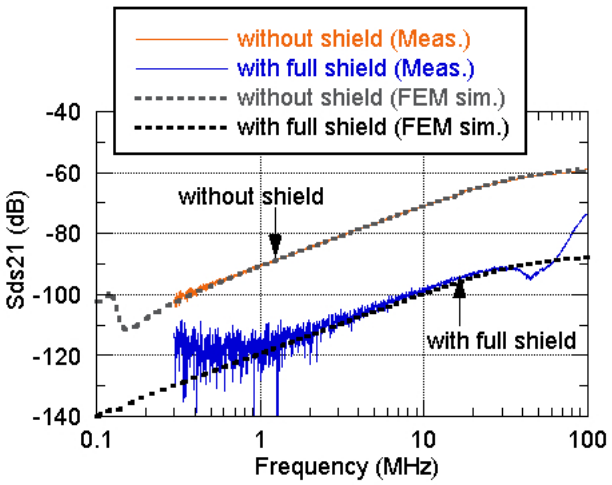

(b) Differential mode coupling

Fig. 11. Comparison between couplings without shield and with full shield. (Solid lines show measurements. Dotted lines show simulations.)

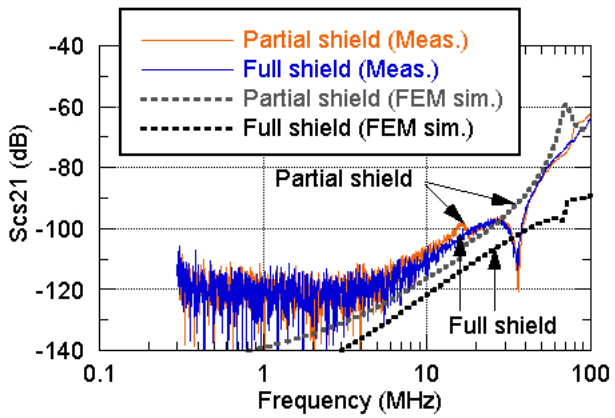

(a) Common mode coupling

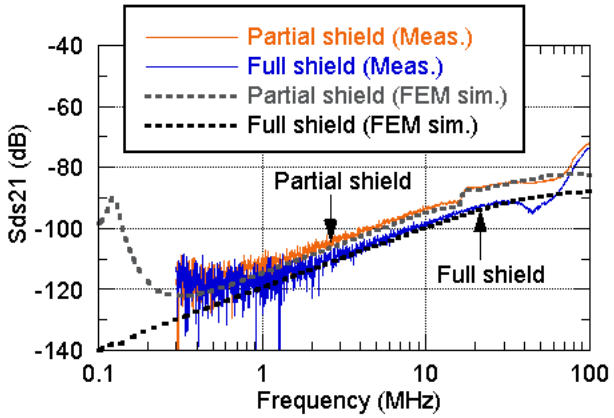

(b) Differential mode coupling

Fig. 12. Comparison between couplings with full shield and with partial shield. (Solid lines show measurements. Dotted lines show simulations.)

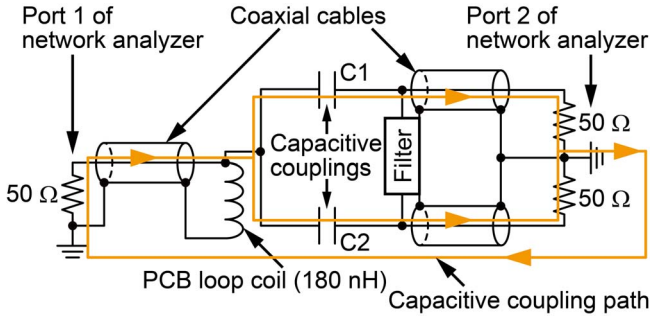

Fig. 13. Capacitive coupling path in Scs21 measurement.

Using an aluminum shielding plate, we measured and simulated the shielding performance against the magnetic couplings. We compared two types of shield. A full shield shown in Fig. 10(b) covers all of the EMI filter. A partial shield shown in Fig. 10(c) covers L_{CMC1} , C_{X1} , C_{Y1} , and busbars connecting between L_{CMC1} and port 2. Figure 11 shows the comparison between couplings without shield and with full shield. Sds21 is reduced about 30 dB by the shield. The simulated Sds21 agrees with the measurement within 5 dB at the frequency lower than 70 MHz. However, the simulated Scs21 is about 15 dB lower than the measurement.

The ground of port 1 and the ground of port 2 are insulated in the simulation, whereas they are connected by the shield of coaxial cables and a metal housing of a network analyzer in the measurement. For this reason, the signal propagates through capacitive couplings C1 and C2 between the PCB loop coil and port 2. Figure 13 shows the capacitive coupling path in the Scs21 measurement. Figure 11 (a) also shows Scs21 simulated by a simple equivalent circuit model. In the circuit model, 180 nH inductance of a PCB loop coil, C1, C2 and 50 ohm resistances of port 1 and port 2 shown in Fig. 13 are considered. When C1 and C2 are 0.05 pF, simulated Scs21 agrees with the measurement. Therefore, the ground of port 1 and the ground of port 2 should be connected to consider the capacitive couplings in the simulation. In order to avoid the effect of coaxial cables, we should connect between the two grounds by a metal component whose inductance is lower than that of coaxial cables.

Figure 12 shows the comparison between couplings with full shield and with partial shield. The simulated Sds21 agrees with the measurement within 5 dB at the frequency lower than 70 MHz. Sds21 with partial shield is only 5~10 dB larger than Sds21 with full shield. Therefore, the area covered by the partial shield is the necessary shielding area. The simulated Scs21 differs from the measurement because of the capacitive coupling path shown in Fig. 13.

V. Measurement of Conducted Emission

Finally, we measured conducted emission generated by an our prototype converter on which the studied EMI filter is mounted. Using a metal shielding plate, we studied how much the shield reduce the conducted emission. Two shield types similar to the full shield and the partial shield shown in Fig. 10(b) and (c) were compared. A photo of the full shielded EMI filter mounted on the prototype converter is shown in Fig. 14. The EMI filter is closely positioned to power electronic circuits to minimize the converter size, so that the near field generated by them couples with the EMI filter.

We measured conducted emission voltage at an artificial network. Figure 15 shows the measured conducted emission. Though the conducted emission exceeds the limit of CISPR 14-1 without shield, it can be reduced lower than the limit by shielding. The partial shield has the enough performance to reduce the conducted emission. The reduction of conducted emission by the shield is about 10 dB. However, it is lower than the 30 dB reduction shown in Fig. 11. The shielding performance is probably degraded because the shielding plate is not electrically connected to the metal housing well. We also measured a common mode factor and a differential mode factor of the conducted emission using a separator [12]. Figure 16 shows the common mode factor and the differential mode factor of the conducted emission without shield. The conducted emission is mainly caused by differential mode couplings to the EMI filter.

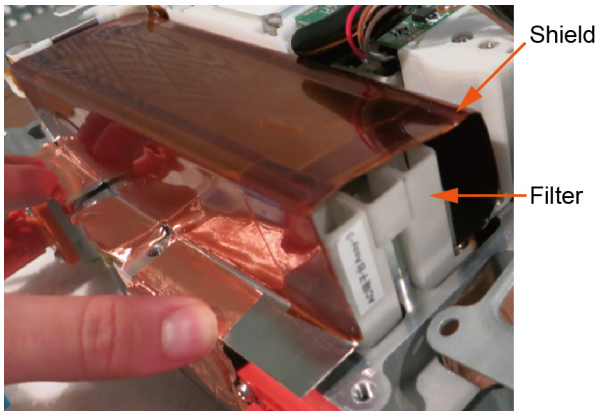

Fig. 14. Photo of a full shielded EMI filter mounted on a prototype converter.

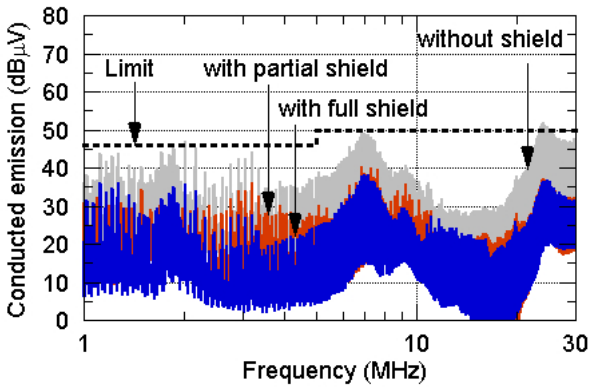

Fig. 15. Measured conducted emission.

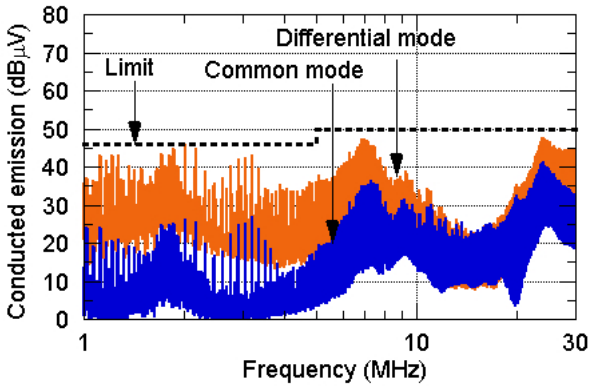

Fig. 16. Measured common mode factor and differential mode factor of conducted emission without shield.

VI. Conclusion

We created an FEM simulation model of an EMI filter which simulates the shielding performance as well as the attenuation performance. The shielding performance was evaluated using a loop coil as an external near field source. Simulated differential mode coupling agreed with the measurement well. We specified the necessary shielding area of the EMI filter using the simulation results. Although the simulated common mode coupling differed from the measurement, the difference will be reduced by connecting the ground of EMI source and the ground of EMI filter to consider the capacitive couplings. A next step is detailed modeling of the EMI source, for example switching devices.

References

[1] N. Oswald, P. Anthony, N. McNeill, and B. H. Stark, "An experimental investigation of the tradeoff between switching losses and EMI generation with hard-switched All-Si, Si-SiC, and All-SiC device combinations," *IEEE Trans. Power Electron.*, vol. 29, no. 5, pp. 2393–2407, May 2014.

[2] S. Wang, F. C. Lee, D. Y. Chen, and W. G. Odendaal, "Effects of parasitic parameters on EMI filter performance," *IEEE Trans. Power Electron.*, vol. 19, no. 3, pp. 869–877, May 2004.

[3] H. Chen, Z. Qian, Z. Zeng, and C. Wolf, "Modeling of parasitic inductive couplings in a Pi-shaped common mode EMI filter," *IEEE Trans. Electromagn. Compat.*, vol. 50, no. 1, pp. 71–79, Feb. 2008.

[4] T. D. Oliveira, J.-M. Guichon, J.-L. Schanen, and L. Gerbaud, "PEEC-Models for EMC filter layout optimization," in *Proc. 6th International conference on Integrated Power Electronics Systems (CIPS 2010)*, Nurnberg, Germany, Mar. 2010.

[5] I. F. Kovačević, T. Friedli, A. Müsing, and J. W. Kolar, "3-D electromagnetic modeling of parasitics and mutual coupling in EMI filters," *IEEE Trans. Power Electron.*, vol. 29, no. 1, pp. 135–149, Jan. 2014.

[6] A. Gheonjian, B. Khvitia, D. Yeremian, Z. Kutchadze, R. Jobava, and X. Bunlon, "Full wave MOM Simulations of EM interactions in EMC filters from 10kHz to 50MHz," in *Proc. 17th International Symposium on ElectroMagnetic Compatibility (CEM2014)*, Clermont-Ferrand, France, June–July 2014.

[7] G. Asmanis, D. Stepins, A. Asmanis, and L. Ribickis, "Mutual couplings between EMI filter components," in *Proc. 2015 Internatioanal Symposyum on Electromagnetic Compatibility (EMC Europe 2015)*, pp. 908–913, Dresden, Germany, Aug. 2015.

[8] *CST Microwave Studio® 2015 – Workflow and solver overview*, CST – Computer Simulation Technology AG, 2015.

[9] Y. Yoshizawa, S. Oguma, and K. Yamauchi, "New Fe-based soft magnetic alloys composed of ultrafine grain structure," *J. Appl. Phys.*, 64, pp. 6044–6046, 1988.

[10] J. Nerg and J. Partanen, "A simplified FEM based calculation model for 3-D induction heating problems using surface impedance formulations," *IEEE Trans. Magn.*, vol. 37, no. 5, pp. 3719–3722, Sep. 2001.

[11] *Nanocrystalline soft magnetic material Finemet® (brochure)*, Hitachi Metals, Ltd., Apr. 2005.

[12] C. R. Paul and K. B. Hardin, "Diagnosis and reduction of conducted noise emissions," *IEEE Trans. Electromagn. Compat.*, vol. 30, no. 4, pp. 553–560, Nov. 1988.